

Tuning the Band Gap Energy of Reduced Graphene Oxide Using Biopolymer Chitosan for High Power and Frequency Device Applications

Solomon L. Joseph¹, Agumba O. John^{1*},
Fanuel K. Mugwang¹, Gabriel G. Katana¹

¹Department of Physics, Pwani University, P. O. Box 195-80108, Kilifi, Kenya

Abstract:

There has been continued research to realize the potential of wide-bandgap (WBG) semiconductors for power switching applications since larger band gap allows higher power and temperature operation and the generation of more energetic (i.e. blue) photons. As compared to other semiconductor materials, reduced graphene oxide (rGO) has a low bandgap energy, which limits its application for high power semiconductors. Blending rGO with chitosan bio-polymer widens its bandgap, which can be tuned by controlling the amount of chitosan. In this study, the interplay between the resultant structure and opto-electronic properties of rGO obtained from coconut husks via thermal pyrolysis blended with chitosan from *squid gladii* have been systematically studied. We thus report that the optical band gap of rGO can be systematically controlled by careful addition of chitosan in their blend. This can give it a new application as high power semiconductors.

Keywords: Chitosan; Reduced Graphene Oxide; Tauc's relation; Optical bandgap energy; Blue shift

Received: January 6, 2019; **Accepted:** January 22, 2019; **Published:** January 28, 2019

Competing Interests: The authors have declared that no competing interests exist.

Copyright: 2019 John AO. This is an open-access article distributed under the terms of the Creative Commons Attribution License, which permits unrestricted use, distribution and reproduction in any medium, provided the original author and source are credited.

***Correspondence to:** Agumba O. John, Department of Physics, Pwani University, P. O. Box 195-80108, Kilifi, Kenya

E-mail: agumba.john@hotmail.com

1. Introduction

There has been up to date research on the acknowledgment of the potential uses of wide-bandgap (WBG) semiconductors for power switching applications. WBG semiconductors are semiconducting materials that can operate at temperatures above 150°C without external cooling, have the potential for longer lifetimes at higher operating voltages, and can switch at higher frequencies with lower power losses. Currently, WBG materials are increasing their importance in many industrial energy-saving technologies and have broad applications in power electronics and solid-state lighting (SSL) [1]. Presently, silicon (Si) is the most widely used in WBG technology. However, Si exhibits some serious limitations i.e., its voltage blocking capability, operation temperature and switching frequency [1, 2]. Therefore, a new generation of materials for power devices applications are required to mitigate the limitations of Si based materials. The use of these new materials in power semiconductor devices will lead to increase in the efficiency of the electric energy transformations, thus achieving a more rational usage of the electric energy. Devising new WBG materials will open a window for new applications and innovations. Reduced graphene oxide is an exciting material since its optical and electronic properties can be controlled by controlling the amount of oxygen functional groups. However, the optical band gap of rGO can be widened effectively to about 2.7eV from 1.15eV [3]. This is still below the bandgap limit for WBG material, which is about 3.5eV to 4.6 eV [4]. Chitosan (a partially N-deacetylated derivative of Chitin) is a polysaccharide consisting of D-glucosamine and N-acetyl-glucosamine units, connected via β -(1→4) glycosidic linkages, derived from Chitin via deacetylation process [5]. Deacetylation of chitin can be approached by several methods, such as alkaline deacetylation [6], enzymatic deacetylation [5], intermittent water washing, flash solvent and organic solvents deacetylation methods [6]. Among all the above mentioned ways, alkaline deacetylation is the most commonly used [7]. The deacetylation process does away with the acetyl groups (-COCH₃) in N-acetyl-D-glucosamine units in Chitin and converts it to D-glucosamine units with no amine groups (-NH₂) to form Chitosan products that are highly soluble in selective weak organic acids due to its relatively high reactivity as compared to the chitin [8].

Heng Zhao *et al* [9] prepared rGO-Ch composite hydrogels through self-assembly of chitosan molecules and rGO. Hui Yuan *et al* [10] synthesized rGO/chitosan nanocomposites for various applications. The new material was found to poses not only large specific surface area and good electrical properties, but also specific functional groups with properties different from those of iron-carbon composite, which has a wide range of industrial applications e.g. capacitors, sensors, catalysts, and electric/thermal conductive composites [11]. Ping Feng and coworkers [12] studied the proton conducting rGO/chitosan composite electrolytes as gate dielectrics for new-concept devices. Solution processed RGO/chitosan composite film was found to be an excellent proton conducting electrolyte with a high specific capacitance of $\sim 3.2 \mu\text{F}/\text{cm}^2$ at 1.0 Hz, and it was used to fabricate multi-gate electric double layer transistors. Reduced graphene oxide (rGO) is a two-dimensional nanostructured combination of carbon and oxygen functional groups obtained after oxidation and reduction of graphene. During the oxidation process, C=C double bonds are broken down and oxygen functional groups, such as -COOH, -OH, and C-O-C, are introduced in the basal plane and at the edges of the graphene sheets [13]. These functional groups are further reduced by chemical, thermal, and electrochemical treatments to form rGO [14]. This material is attractive for a wide range of technological applications due to its tunable chemical [15] and atomic properties. In particular, chemical tuning of rGO via chemical reduction is a growing area in the current research [16]. One possible way to exploit these functionalities is to use rGO to create composite materials. Incorporating rGO sheets into correlated-electron materials offer a new pathway for tailoring their properties [17]. A

lot has been done on tuning the mechanical and electrical properties of rGO by blending it with chitosan. Little has been studied on the optical properties of rGO/chitosan composite, including the optical bandgap energy, and how it can vary by controlling the amount of chitosan within the composite material. In this research, we were able to tune the morphology of rGO using chitosan as a filler which resulted in a wider optical bandgap, thus improving its potential application as a WBG material, with an intention of replacing Si, which up to date, is being applied as a WBG material in many applications, despite its serious limitations i.e., its voltage blocking capability, operation temperature and switching frequency.

2. Materials and Methods

In this study, the materials used were extracted from the locally available biomass wastes. rGO was obtained via thermal pyrolysis of coconut husks, which chitosan was extracted from *squid gladii* via chemical synthesis. The absorption spectra were obtained using Agilent Technologies Carry 60 UV-Vis spectrophotometer while the optical microscopy was done using Motic microscope fitted with Moticam 3.0 camera.

2.1. Reduced Graphene Oxide Synthesis

rGO was obtained via thermal decomposition of coconut husks biomass waste. The husks were cleaned using running water, to remove external dirt and dust. This was followed by drying in the sun for four days to remove moisture. The dried husks were further dried in a hot air oven at about 60⁰C for 6 hours to aid for further removal of moisture. The dry husks were grounded into fine powder (1.5 mm). 15 g of the powder was put in a crucible, covered with crucible lid and then wrapped in three layers of aluminum foil to prevent oxidation during the carbonation process. The wrapped samples were put in a hot furnace at about 100⁰C for 5 hours [19]. A black powder, graphite, was obtained. The graphite powder was oxidized thermally in a 500⁰C hot furnace for 5 hours to obtain reduced graphite oxide. A brownish powder was obtained. 0.1 g of the powder was mixed with 10 ml distilled water in a glass vial. The mixture was sonicated at 25 kHz for 30 min to exfoliate rGO. The solution was filtered using 0.45 Polytetrafluoroethylene (PTFE) filters to remove un-exfoliated graphite and other debris [18].

2.2. Chitosan Extraction

Four stages were followed during chitosan extraction process. They are pre-treatment stage, demineralization, deprotonation and deacetylation stages. The squid gladii were collected along the Kilifi coastal beaches (Kenya) and washed to remove external matter. This was followed by sun drying for four days. 10 g of the dry gladii were soaked in 50 ml of 0.01M NaOH at room temperatures for about 1 hour to remove non-chitin rich organic material. Here, also a small amount of proteins were also removed during this stage. The pre-treated squid gladii were washed and sundried for two days then grounded into fine powder (1.5 mm). 8 g of powder was soaked in 80 ml of 1MHCl solution at a temperature of about 60⁰C for 3 hours to dissolve minerals. The Demineralized powder was filtered off the acidic solution and washed in distilled water to remove the acid. The deprotonation process was aided to remove the proteins from the demineralized gladii powder. This was done by soaking the washed powder in 0.125M NaOH at 70⁰C overnight. Once the deprotonation step was complete and successful, the remaining component was the biopolymer chitin. The base was washed off the chitin powder using distilled water, then filtered to obtain chitin powder. The filtered chitin was dried in a hot air oven at 60⁰C for about 5 hours. The final step was deacetylation; conversion of chitin to chitosan.

This was achieved by boiling the demineralized chitin powder in of 1.25M NaOH at a 100 °C for six hours. This was repeated thrice to obtain high deacetylated chitosan. The powder was then washed severally in distilled water until neutral pH. A white solid, chitosan, was obtained. The extracted chitosan was washed in alcohol to dissolve any non-chitosan compound. 0.01 g of the extracted chitosan was dissolved in 1% acetic acid and left to shake overnight in a warm water bath (about 50 °C).

2.3. rGO-Ch Composite Samples Preparation

During the composite forming process, Here, 1 ml of rGO solution each was measured into 4 clean glass vials labeled A, B, C and D. To vial A, 0.5 ml of chitosan solution was added to make 33% chitosan blend, 1 ml of chitosan solution to vial B (50% chitosan), 1.5 ml of chitosan of chitosan solution to vial C (60% chitosan) and lastly 0.25 ml of chitosan solution was added to vial D (20% chitosan). The four vials were left shaking for 3 hours under a water bath at 50 °C [20].

2.4. The Optical Spectroscopy

The absorption spectra of the pure and blend solutions were measured using Agilent Technologies Carry 60 UV-Vis spectrophotometer within the range of 200 nm to 500 nm at 1 nm interval. The spectra were then analysed using Microcal Origin Pro. The Optical band gaps (E_g) obtained from the use of *Tauc's relation*.

3. Results and Discussion

3.1. Morphologies of the Solution Structures

The micrographs in Figure 1 were obtained from thin films for 20%, 33%, 50% and 60% chitosan ratio in rGO/Chitosan blend solutions as presented by Figures 1 (a), (b), (c) and (d) respectively. The films of the blend solution were prepared by sliding method on a glass slide as suggested by Deng and coworkers [21]. Nucleation due to shearing forces occurred during the sliding process which resulted in formation of dendritic structures. According to the crystal growth theory, dendrites are formed in the diffusion field crystal growth. This occurs when part of the seed grows faster than the other due to the concentration gradient. The most favored part grows faster due to high diffusion gradient, leading to uneven growth (deformations). As a result, the flat seed becomes unstable, leading for formation of dendrites. The structures in Figure (1a) were smaller in size (20% chitosan ratio). This was due to low solution temperatures and high nuclei density. Dendritic crystals were formed due to growth instabilities that occur when the growth rate is limited by the rate of diffusion of molecules to the growth front. For low concentration of chitosan in the blend, the nucleation density was higher which brought about competitions for the few available chitosan molecules. On increasing the density of chitosan molecules and letting the nucleus density to remain constant, there was enough room for molecules to diffuse freely in solution, looking for a most favored diffusion gradient. This resulted in a fewer structures, but larger in size, as shown in Figure 1 (b, c, d). As the chitosan ratio increased further, the structures grew bigger. When the chitosan ratio in the blend was lower than that of rGO, i.e 20% {Figure (a)}, the structures were many, but smaller in size. This could be due to the fact that the higher ratio of rGO provided many seeds, on which the few available chitosan molecules got attached, thus resulting into small structures. As the ratio of chitosan was increased, the structures became few, but grew larger in size.

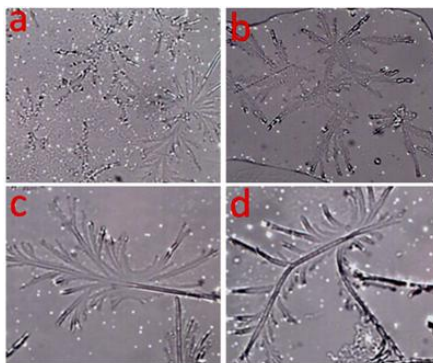


Figure 1 Micrographs of rGO/Chitosan blend solutions prepared on glass slides using sliding method with different chitosan ratios. Figure (a) shows the micro-structures for 20% chitosan ratio, (b) represents 33%, (c) is for 50% while (d) is the micrograph for 60%. All the micrographs were taken at room temperatures. (Image sizes are 150 X 125 μm).

3.2. Optical Spectroscopy

3.1.1. Optical Spectra of rGO

The absorbance spectrum from a solution of rGO was recorded between a range of 200 nm to 500 nm wavelength at 1 nm interval (Figure 2). To understand the extend and be able to identify the peaks (Figure 2a), the data was deconvoluted (figure 2a) using multi-Gaussian fits. The black bold line represents the raw data and the bold red is the fit while blue and dark cyan shows the deconvoluted peaks (Figure 2). It was observed that rGO had maximum absorbance at *ca* 277.6 nm for P_1 and *ca* 231.0 nm for P_2 . This is in close agreement with literature. The peak at *ca* 231 nm in the absorption spectra of graphene oxide maybe associated with to π - π^* transitions of the aromatic C–C bond [22] and a shoulder at *ca* 278 nm correspond to n - π^* transition of the C=O bond [23]. The FWHM for P_2 was found to be *ca* 112.8 nm while for P_1 was *ca* 59.6 nm.

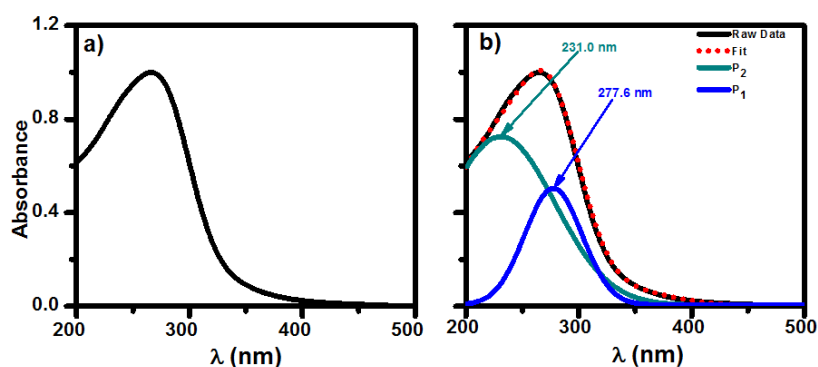


Figure 2 Absorbance spectra for rGO solution within wavelength range of 200 nm to 500 nm. Figure (a) shows the normalized raw data spectrum while Figure (b) shows the spectra obtained after convolution. In Figure (b), black spectrum represents the raw data {same spectra as one in Figure (a), red one is its fit while blue and dark cyan represents the convoluted peaks .after fitting. P_1 had a maximum absorbance at *ca* 277.6 nm while P_2 had a maximum absorbance at *ca* 231 nm. All the spectra were measured at room temperature.

3.3. Optical Absorption of Chitosan Solution

Figure 3 shows the UV-Vis absorption spectrum for chitosan solution measured at room temperature.

The data was then normalized (Figure (3a)) and deconvoluted (Figure (3b)). Figure (3a) shows the normalized raw data spectrum for chitosan solution while Figure (3b) shows the spectra obtained after deconvolution where, blue spectrum represents the raw data, and blue and black representing the deconvoluted peaks.

Peaks P_1 and P_2 had a maximum absorbance at 236 nm and at 203 nm respectively. The peak at 236 nm (Figure 3b) could attributed to n- σ^* transition of amine free electrons [24]. The FWHM for peak P_2 was 10.2 nm while for peak P_1 was 167.6 nm. We further compared the absorption spectra for rGO and chitosan. Figure 4 show the P_1 spectra for rGO and chitosan. We observed that both materials absorbed strongly within the UV region of the absorption spectrum. rGO absorbs at 277.6 nm while Chitosan absorbs at 231.0 nm, which suggested that high photon energy is required to excite an electron from ground state to higher excited state. The FWHM for rGO was 59.6 nm while the one for Chitosan was 167.5 nm. The large chitosan FWHM was attributed to a wide distribution of crystal domains (wide distribution of absorbing chromophores)

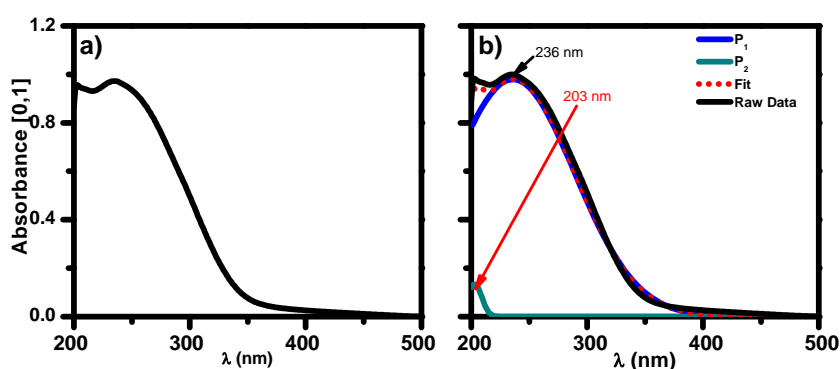


Figure 3 Absorbance spectra for chitosan measured at room temperature within wavelength range of 200 nm to 500 nm. Figure (a) shows the normalized raw data spectrum for chitosan while Figure (b) shows the spectra obtained after deconvolution. In Figure (b), blue spectrum represents the raw data {same spectra as one in Figure (a), green one is its fit while black and red represents the convoluted peaks after fitting. P_1 had a maximum absorbance at 236 nm while peak P_2 had a maximum absorbance at 203 nm.

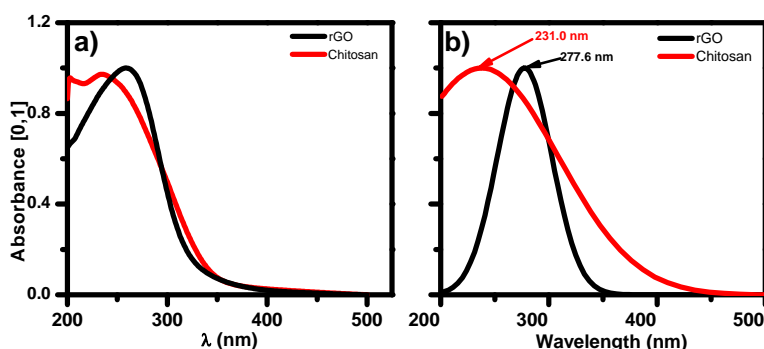


Figure 4 Comparison between UV-Vis spectra for rGO and Chitosan. Figure (a) shows the raw normalized spectra while Figure (b) are the convoluted spectra. It was found that rGO absorbs at 277.6 nm while Chitosan absorbed at 231.0 nm.

3.4. The Effect of Chitosan Ratio on rGO Absorbance Spectrum

From the discussion above, chitosan chromophores are widely distributed towards the blue region of

the absorption spectrum. The broad peak implied that absorbance took place over a wide distribution of absorbing units. This phenomena can be attributed to different levels of order within the matrix of the polymeric chains. Blending a polymer with a carbon based material initiate polymer crystallization via induced nucleation. Once nucleation initiated, structural growth takes over. We found out that rGO has a maximum absorbance wavelength at 277.6 nm while chitosan has a maximum absorbance at 231.0 nm. It can be seen that chitosan chromophores absorbs within the bluer region than rGO.

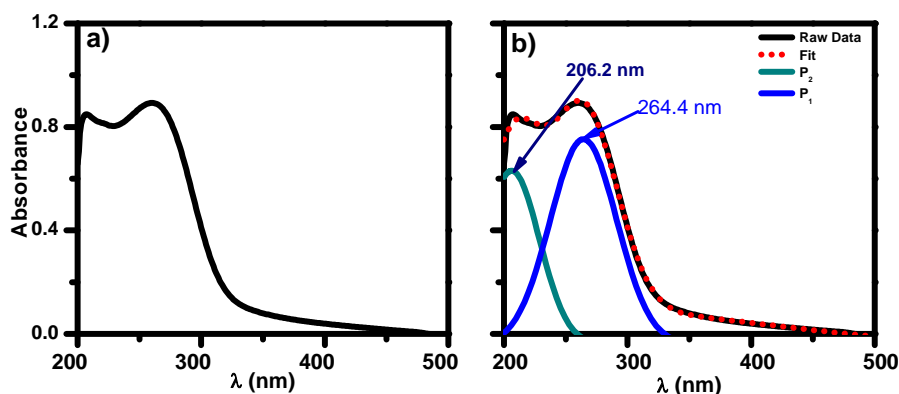


Figure 5 Absorbance spectra for blend solution A, which had the ratio of rGO:Chitosan as 2:1, (33% Ch) within wavelength range of 200 nm to 500 nm at room temperature. Figure (a) shows the normalized raw data spectrum for blend A while Figure (b) shows the spectra obtained after deconvolution. In Figure (b), black spectrum represents the raw data {same spectra as one in Figure (a), red one is its fit while blue and dark cyan represents the convoluted peaks after fitting. P_1 had a maximum absorbance at 264.4 nm while peak P_2 had a maximum absorbance at 206.2 nm.

Figure 5 shows the normalized absorbance spectra for blend A (33% Ch), with ratio of rGO:Chitosan as 2:1. The peaks P_1 had a maximum absorbance at *ca* 264.4 nm while peak P_2 had a maximum absorbance at *ca* 206.2 nm. The FWHM for P_2 peak was at *ca* 63.4 nm while that one for P_1 was at *ca* 52.8 nm. From the data, it was observed that the rGO low energy peak (P_1) shifted from 277.6 nm to 264.4 nm after forming a blend comprising of 33% chitosan.

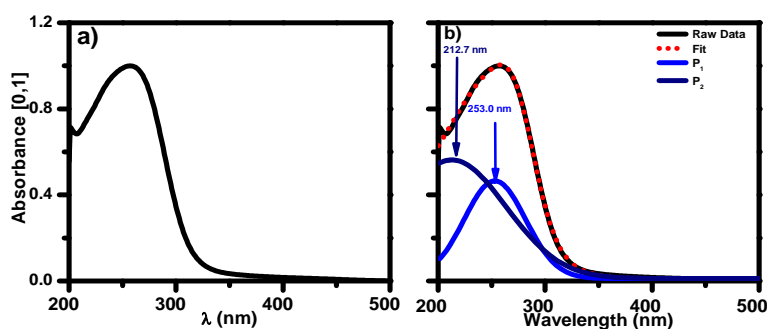


Figure 6 Absorbance spectra for blend B, which had the ratio of rGO:Chitosan as 1:1, within wavelength range of 200 nm to 500 nm. Figure (a) shows the normalized raw data spectrum for blend B while Figure (b) shows the spectra obtained after convolution. In Figure (b), black spectrum represents the raw data {same spectra as one in Figure (a), red one is its fit while blue and dark cyan represents the deconvoluted peaks after fitting. P_1 had a maximum absorbance at 253.0 nm while P_2 had a maximum absorbance at 212.7 nm.

The ratio of chitosan within the blend was increased to 50%, and the spectra as shown in

Figure 6 were obtained. In this blend, the ratio of rGO:Chitosan was 1:1. The deconvoluted peaks show P_2 had a maximum absorbance at 253.0 nm while peak P_1 had a maximum absorbance much below the scanning range, which was ca 212.7 nm. The FWHM for peak P_1 was found to be ca 67.6 nm and ca 119.4 nm for P_2 . The P_1 peak was further blue shifted to 253.0 nm

The chitosan ratio was lastly increased to 60%. Blend C (60% Ch) had a high ratio of chitosan compared to rGO, i.e., 2:3 (rGO:Chitosan). Figure 7 shows the absorbance spectra for blend C. In Figure 7 (a) shows the normalized raw data spectrum for blend C while (b) are the spectra obtained after deconvolution. In Figure (7b), black spectrum represents the raw data {same spectra as one in Figure 7 (a), red one is its fit while blue and dark cyan represents the convoluted peaks after fitting. The peak P_1 had a maximum absorbance at 249.4 nm while peak P_2 had a maximum absorbance outside the scanned range, at ca 118.9 nm. The separation between the peaks was about 9.5 meV. The FWHM for peak P_1 was obtained as ca 85.9 nm and ca 87.1 nm for P_2 .

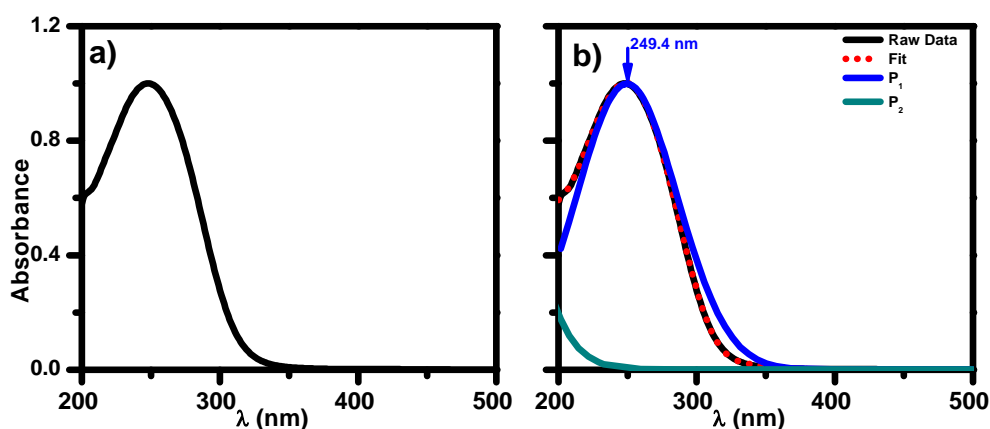


Figure 7 Absorbance spectra for blend C (60% Ch), which had the ratio of rGO:Chitosan as 2:3, within wavelength range of 200 nm to 500 nm. Figure (a) shows the normalized raw data spectrum for blend B while Figure (b) shows the spectra obtained after deconvolution. In Figure (b), black spectrum represents the raw data {same spectra as one in Figure (a), red one is its fit while blue and dark cyan represents the deconvoluted peaks after fitting. P_1 had a maximum absorbance at 249.4 nm while P_2 had a maximum absorbance outside the scanned range. The measurements were done at room temperature.

We now compared the low energy peaks (P_1) for pure Chitosan, pure rGO and for the three blends with different chitosan ratios, to visualize the effect of increasing chitosan ratio on the rGO absorption spectrum. Figure 8 shows their normalized raw ((Figure 8(a)) and deconvoluted spectra for rGO ((Figure 8(a)). The black spectra represent rGO spectrum, red is for chitosan, while blue, green and magenta represents the spectrum for blends A, B and C respectively. It can be observed that increasing chitosan ratio, the peaks got blue shifted. Since chitosan absorbed at bluer region as compared to rGO, then addition of more chitosan chromosomes over dominated the ones for rGO, which were kept constant. This resulted to blue shifting of rGO peak, from 278 nm to a lower value depending on the chitosan ratio. Chitosan peak was found to be broader than the one for rGO. This can be attributed to a wider distribution of crystal domains within the chitosan structures, which required high photon energy to promote an electron to a higher excited state. Adding more of these domains resulted in widening of the rGO peak. In summary, it was obtained that increasing the chitosan ratio resulted in a blue shifting of rGO peak, which got broadened at the same time.

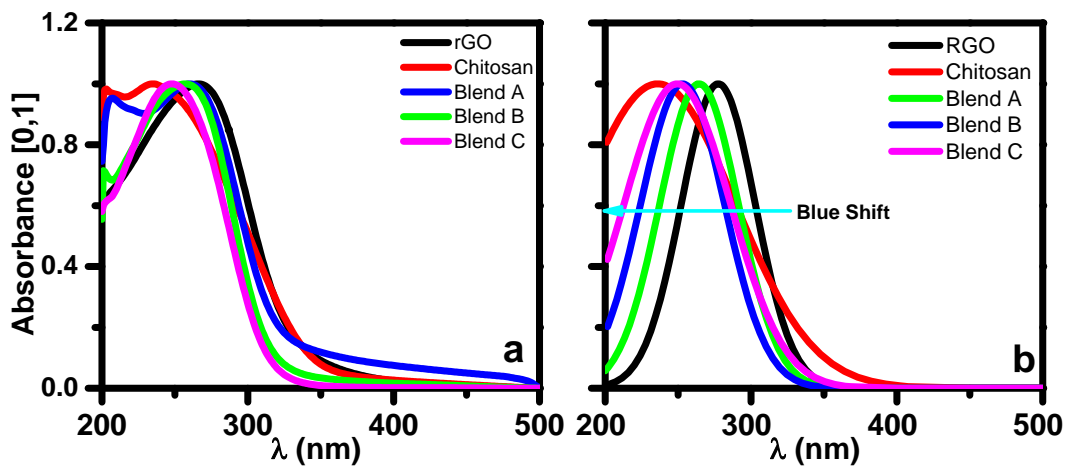


Figure 8 Normalized spectra for rGO, chitosan and their blends at different chitosan ratio. Figure (a) shows the raw data spectra while Figure (b) represents their respective P_1 peaks after convolution. The black represent rGO spectrum, red is for chitosan, while blue, green and magenta represents blends A, B and C respectively. It can be seen that increasing chitosan ratio, the peaks blue shifted.

3.5 The Effect Concentration on the Optical Band Energy

The optical absorption is dominated by the optical band gap (E_g) of the semiconductor that is related to the optical absorption coefficient (α) and the incident photon energy $h\nu$ by using *Tauc equation* (Equation 1).

$$\alpha h\nu = A(h\nu - E_g)^n \quad (1)$$

In this equation, α is absorption coefficient, A is constant that is independent from ν and n the exponent that depends on the kind of optical transition. This constant can be $\frac{1}{2}$ when the transition is direct-allowed and 2 when it is indirect- allowed. In this experiment, the value of n was found to be 2 (which corresponds to indirect band to band transition) because that value of n yields the best linear graph of $(\alpha h\nu)^{0.5}$ verses $h\nu$ for rGO and all blends and $\frac{1}{2}$ for Chitosan (Chitosan has direct band gap [25]). The photon energy is given by $h\nu$. The intersection of the straight line with the $h\nu$ -axis determines the optical band gap energy E_g . According to Shujahadeen, the E_g for chitosan ranges from 3.7 eV to about 5.3 eV depending on the purity and DDA [25], while for rGO ranges from 1.4 eV to about 3.3 eV depending on the concentration of oxygen molecules [26]. The direct allowed energy band gap (E_g) must be overcome for the electronic transition from the upper level of valence band and the lower level of conduction band.

Using the *Tauc's model*, we were able to estimate the energy bandgap energy as shown in Figure 9. It was observed that there was an increase in the optical bandgap energy with increase in the chitosan ratio. This was attributed to blue shifting and broadening of the rGO absorption peaks, as discussed above. From the study, we observed that the bandgap energy of rGO can be widened by blending it with chitosan. To suit a particular WBG application, the wide bandgap can be tuned to the required value by varying the amount of chitosan.

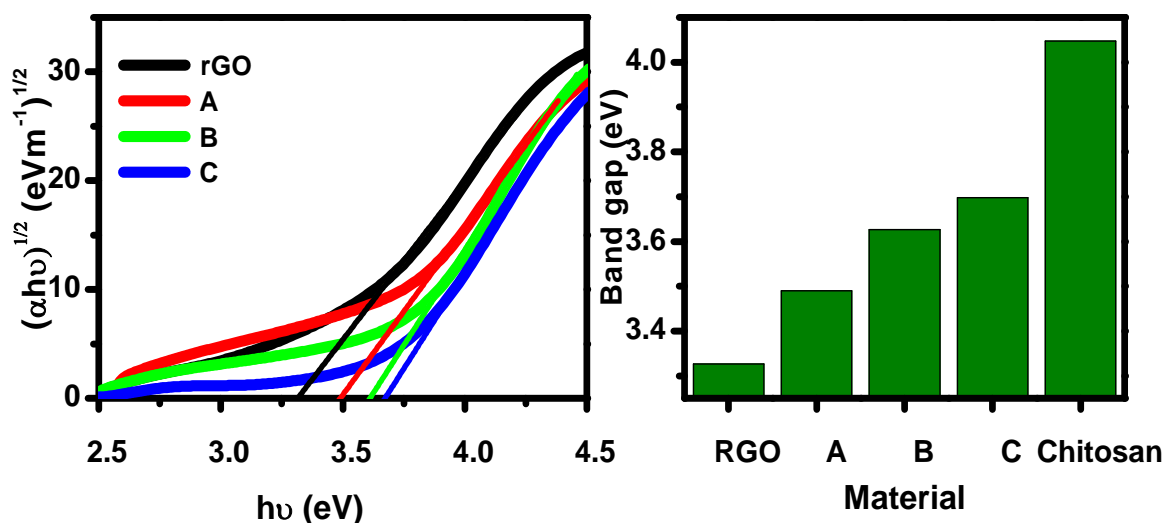


Figure 9 The relationship between $(\alpha h\nu)^{1/2}$ (eV m^{-1})^{1/2} versus $h\nu$ (eV) and the optical band gap energy (E_g) for rGO and the blends of rGO:Ch for A(33% Ch), B(50% Ch) and C(60% Ch).

4. Conclusions

In this work, we have investigated the influence of the chitosan ratio in the blend with reduced graphene oxide on the absorption spectra and on the optical band gaps (E_g). From this study, we report that both the materials absorb in the UV region with chitosan displaying a broader and blue shifted spectra. The absorption spectra of the blend got blue shifted with increase of the chitosan ratio within the blend. Furthermore, the optical band gap of rGO increased by carefully adding controlled amounts of chitosan in their blend. This result could open opportunities in high temperature conductivity, high power and high frequency device applications.

Acknowledgements

We would like to extend our sincere gratitude to Pwani University fraternity for availing basic equipment for this research. We would further appreciate all colleagues from the department of Physics and the school of pure and applied sciences, who supported us during our research through various discussions and seminar presentations.

References

1. Jos é M, Philippe G, Amador PT. Wide Band Gap Semiconductor Devices for Power Electronics. *ATKAF*. 2012, 53:107-116
2. Jose M, Xavier P, Amador P, Jos ´e R. A Survey of Wide Bandgap Power Semiconductor Devices. *IEEE Transactions on Power Electronics*. 2014, 59:2155-2163
3. Velasco-Soto MA, Pe ´rez-Garcı ´ SA, Alvarez-Quintana J, Cao Y, Nyborg L, Licea-Jime ´nez L. Selective band gap manipulation of graphene oxide by its reduction with mild reagents Selective band gap manipulation of graphene oxide by its reduction with mild reagents. *Carbon N. Y.* 2015, 93:967-973

4. Millan J, Godignon P, Perpina X, Perez-Tomas A, Rebollo J. A survey of wide bandgap power semiconductor devices. *IEEE Trans. Power Electron.* 2014, 29:2155-2163
5. Tsigos I, Martinou A, Kafetzopoulos D, Bouriotis V. Chitin deacetylases : New Versatile Tools in Biotechnology,” *TIB Technol.* 2000, 18:305-312
6. Maria M, Gadelha S, Stamford TCM, Pereira E, Ten ório P, Sampaio F. Chitosan as an oral antimicrobial agent. *Sci. against Microb. Pathog. Commun. Curr. Res. Technol. Adv.* 2011, 542-550
7. Cheung RC, Ng TB, Wong JH, Chan WY. Chitosan: An Update on Potential Biomedical and Pharmaceutical Applications. *Mar. Drugs.* 2015, 13:5156-5186
8. Sugiyanti D, Darmadji P, Anggrahini S, Anwar C, Santoso U. Preparation and Characterization of Chitosan from Indonesian Tambak Lorok Shrimp Shell Waste and Crab Shell Waste. *Pakistan J. Nutr.* 2018, 17:446-453
9. Zhao H, Jiao T, Zhang L, Zhou J, Zhang Q, Peng Q. Preparation and adsorption capacity evaluation of graphene oxide-chitosan composite hydrogels. *Sci. China Mater.* 2015, 58:811-818
10. Yuan H, Meng L, Park S. A review : synthesis and applications of graphene/chitosan nanocomposites. *Carbon Lett.* 2016, 17:11-17
11. Feng Y, He C, Wen Y, Ye Y, Zhou X, Xie X, Mai YW. Superior flame retardancy and smoke suppression of epoxy-based composites with phosphorus/nitrogen co-doped graphene. *J. Hazard. Mater.* 2018, 346:140-151
12. Ping F, Peifu D, Changjin D, Yi S, Qing W. Proton Conducting Graphene Oxide/Chitosan Composite Electrolytes as Gate Dielectrics for New-Concept Devices. *Nat. Publ. Gr.* 2016, 6:1-9
13. Kumar N, Srivastava VC. Simple Synthesis of Large Graphene Oxide Sheets via Electrochemical Method Coupled with Oxidation Process. *ACS Omega.* 2018, 3:10233-10242
14. Dong L, Yang J, Chhowalla M, Loh KP. Synthesis and reduction of large sized graphene oxide sheets. *Chem. Soc. Rev.* 2017, 46:7306-7316
15. Jijo A, Kalangi SV, Christopher DW, Kalon G, Yang S, Christie TC, James D, Eric P, Sarah JH, Irina VR, Paola C, Andre KG, Rahul RN. Tunable sieving of ions using graphene oxide membranes. *Nat. Nanotechnol.* 2017, 12:546-550
16. Gupta B, Kumar N, Panda K, Kanan V, Joshi S, Visoly-Fisher I. Role of oxygen functional groups in reduced graphene oxide for lubrication. *Sci. Rep.* 2017, 7:1-14
17. Yeoh WK, Cui XY, Gault B, De Silva KSB, Yen HW, Wong D, On the roles of graphene oxide doping for enhanced supercurrent in MgB₂ based superconductors. *Nanoscale.* 2014, 6:6166-6172
18. Sulistyani E, Boi D, Wulandari F, Budi E. Coconut Shell Activated Carbon as an Alternative Renewable Energy. *Renew. energy Energy Conserv. Exhibition.* 2015, 2:76-81
19. Wardhani K, Nugraha IMA, Abidin S, Ali M, Fahmi A. Solution of Reduced Graphene Oxide Synthesized from Coconut Shells and Its Optical Properties. *AIP 3rd Int. Conf. Adv. Mater. Sci. Technol.* 2017, 020045:1-8.
20. Xu S, Zhang Y, Dong K, Wen J, Zheng C, Zhao S. Electrochemical DNA Biosensor Based on Graphene Oxide- Chitosan Hybrid Nanocomposites for Detection of Escherichia Coli O157 : H7. *Int. J. Electrochem. Sci.* 2017, 12:3443-3458
21. Xiujian Z, Liming H, Xiuzhen X, Liang W, Jincheng W, Qixun S, Shuit - Tong L,

- Jiansheng J. Aligned Single-Crystalline Perovskite Microwire Arrays for High-Performance Flexible Image Sensors with Long-Term Stability. *Adv. Mater.* 2016, 28:2201-2208
22. Wong CPP, Lai CW, Lee KM, Abd HSB. Advanced chemical reduction of reduced graphene oxide and its photocatalytic activity in degrading reactive black 5. *Materials (Basel)*. 2015, 8:7118-7128
23. Chang BY, Huang NM, An'amt MN, Marlinda AR, Norazriena Y, Muhamad MR, Harrison I, Lim HN, Chia CH. Facile hydrothermal preparation of titanium dioxide decorated reduced graphene oxide nanocomposite. *Int. J. Nanomedicine*. 2012, 7:3379-3387
24. Hassan MA, Omer AM, Abbas E, Baset WMA, Tamer TM. Preparation, physicochemical characterization and antimicrobial activities of novel two phenolic chitosan Schiff base derivatives. *Sci. Rep.* 2018, 8:1-14
25. Aziz SB. Morphological and Optical Characteristics of Nano-Composites: Optical Dielectric Loss as an Alternative Method for Tauc's Model. *Nanomaterials*. 2017, 7:1-15
26. Lian K, Ji Y, Li X, Jin M, Luo Y. Big Bandgap in Highly Reduced Graphene Oxides. *J. Phys. Chem. C*. 2013, 117 :6049-6054